

Electronic structure and electron–molecular vibration interaction in dimerized $[\text{Pd}(\text{dddt})_2]_2X$ (where $X = \text{AuBr}_2, \text{SbF}_6, \text{TeCl}_x$) salts studied by IR spectroscopy

Andrzej Łapiński* and Roman Świetlik

Institute of Molecular Physics, Polish Academy of Sciences, Smoluchowskiego 17, 60-179 Poznań, Poland

(Received 22 June 1998; revised manuscript received 15 October 1998)

Polarized reflectance spectra of three isostructural charge-transfer salts $[\text{Pd}(\text{dddt})_2]_2X$ (where $X = \text{AuBr}_2, \text{SbF}_6, \text{TeCl}_x, x = 5$ or 6 , and $\text{dddt} = 5,6$ -dihydro-1,4-dithiin-2,3-dithiolate ligand) have been measured in the frequency range 650 to $40\,000\text{ cm}^{-1}$ at room temperature. Moreover, we studied absorption spectra (400 to $40\,000\text{ cm}^{-1}$) as well as Fourier transform near-infrared Raman spectra of $[\text{Pd}(\text{dddt})_2]_2\text{TeCl}_x$ powders. All the compounds contain strongly dimerized $\text{Pd}(\text{dddt})_2$ stacks. The nature of electronic bands is discussed. A plasma-edge-like dispersion in $[\text{Pd}(\text{dddt})_2]_2\text{AuBr}_2$ and $[\text{Pd}(\text{dddt})_2]_2\text{SbF}_6$ crystals is analyzed in terms of Drude-Lorentz model. The band-structure parameters are determined by assuming a one-dimensional tight-binding model. Deviations between the experimental data and expectations of a one-electron model suggest considerable contributions of electron-electron and electron-phonon interactions to the electronic structure of the materials. The coupling of electrons with the totally symmetric $\text{C}=\text{C}$ vibrations of $\text{Pd}(\text{dddt})_2$ (a_g modes) in $[\text{Pd}(\text{dddt})_2]_2\text{AuBr}_2$ and $[\text{Pd}(\text{dddt})_2]_2\text{SbF}_6$ salts is discussed in terms of an isolated dimer model and the suitable electron-phonon coupling constants are determined. The origin of a_g phonon mode splitting is considered. [S0163-1829(99)06123-8]

I. INTRODUCTION

The organic donor bis(ethylenedithio)tetrathiafulvalene (BEDT-TTF or ET) and various acceptors form the most numerous group of presently known organic conductors and superconductors.¹ In the search for new interesting charge-transfer salts exhibiting high-electrical conductivity many modifications of BEDT-TTF molecule were synthesized. The square planar metal complexes $M(\text{dddt})_2$ (where $M = \text{Ni}, \text{Pd}, \text{Pt}, \text{Au}$, and $\text{dddt} = 5,6$ -dihydro-1,4 dithiin-2,3-dithiolate ligand)^{2,3} are structurally very similar to BEDT-TTF since the only difference lies in that the central $\text{C}=\text{C}$ bond in BEDT-TTF is replaced by a metal (Fig. 1). The $M(\text{dddt})_2$ donors and various inorganic acceptors were successfully used for preparation of many organic metals and semiconductors.^{4–11} In the group of $\text{Pd}(\text{dddt})_2$ and $\text{Ni}(\text{dddt})_2$ salts there exist crystals that preserve metallic properties down to the lowest temperatures but none of them exhibits superconductivity.^{7,9–11} The BEDT-TTF and $M(\text{dddt})_2$ salts with the same anions often possess very similar crystal structures but their physical properties can be quite different. The series of charge-transfer salts based on $M(\text{dddt})_2$ is the second large group of conducting materials based on the transition-metal complexes. Up to now the most attention has been paid to molecular conductors yielded by metal complexes $M(\text{dmit})_2$ (where $M = \text{Ni}, \text{Pd}, \text{Pt}, \text{Au}$, and $\text{dmit} = 4,5$ -dimercapto-1,3-dithiole-2-thione ligand).¹² In this group three $\text{Ni}(\text{dmit})_2$ and three $\text{Pt}(\text{dmit})_2$ salts exhibit superconductivity under pressure and one $\text{Ni}(\text{dmit})_2$ salt becomes superconductor at ambient pressure. A specific feature of the discussed charge transfer salts is the presence of conducting layers formed by BEDT-TTF, $M(\text{dddt})_2$, or $M(\text{dmit})_2$ molecules alternating with the insulating layers of acceptors in BEDT-TTF and $M(\text{dddt})_2$ salts, or donors in the case of $M(\text{dmit})_2$ salts.

Usually, the molecules yielding conducting charge-transfer salts exhibit a relatively large splitting between the highest occupied (HOMO) and the lowest unoccupied (LUMO) molecular orbitals. For example, in BEDT-TTF the energy gap between HOMO and LUMO is about 2 eV and the partially filled valence bands are only derived from one kind of molecular orbital leading to the so-called “one-band systems.” The HOMO and LUMO of $M(\text{dddt})_2$ and $M(\text{dmit})_2$ are very similar in orbital character and for both molecules the energy difference between HOMO and LUMO is relatively small (about 0.4 eV),^{3,13,14} therefore, for the adequate description of the conduction band in the salts formed by these molecules both HOMO and LUMO orbitals have to be taken into account yielding the so-called “two-band systems.”^{15–17} For example, in the case of $M(\text{dddt})_2$ or $M(\text{dmit})_2$ dimers the valence orbitals are given by the in-phase and out-of-phase combinations of the HOMO orbitals (i.e., HOMO^+ and HOMO^-) and the LUMO orbitals (i.e., LUMO^+ and LUMO^-). Consequently, in the conducting layer consisting of such dimers the four valence levels of each dimer yield four bands. The valence bands are formed by strong $\text{S}\cdots\text{S}$ contacts. The filling of these bands depends on the number of electrons in the valence orbitals and the strength of interaction between molecules in dimer.

The spectroscopic methods, especially in infrared (IR) region, are very useful for investigations of crystalline organic conductors providing information about electronic structure, electron-electron and electron-phonon interactions.¹⁸ How-

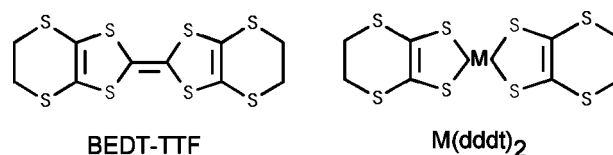


FIG. 1. Molecular structure of BEDT-TTF and $M(\text{dddt})_2$

ever, despite the fact that so many interesting crystals are discovered in the $M(\text{dddt})_2$ family, to our knowledge relatively few optical studies have been performed.^{19–22} In this paper, we present the studies of polarized reflectance spectra of three crystals formed by $\text{Pd}(\text{dddt})_2$ donors and linear (AuBr_2) or octahedral (SbF_6 and TeCl_x , $x=5$ or 6) anions. The $[\text{Pd}(\text{dddt})_2]_2\text{TeCl}_x$ ($x=5$ or 6) is a stable metal down to the helium temperature ($\sigma_{RT}=11\text{--}25\ \Omega^{-1}\text{cm}^{-1}$), the $[\text{Pd}(\text{dddt})_2]_2\text{SbF}_6$ undergoes a metal-insulator phase transition at $T_{M-I}=200\ \text{K}$ ($\sigma_{RT}=1\text{--}2\ \Omega^{-1}\text{cm}^{-1}$) and the $[\text{Pd}(\text{dddt})_2]_2\text{AuBr}_2$ exhibits semiconducting properties ($\sigma_{RT}=2.0\ \Omega^{-1}\text{cm}^{-1}$).⁹ The HOMO-LUMO gap in $\text{Pd}(\text{dddt})_2$ equals to $0.40\ \text{eV}$,¹³ what gives rise to the “two-band structure” in the studied systems. Some preliminary spectroscopic data have been published in Ref. 22.

It is known that the Pd ions tend to form metal-metal bonds; therefore, most of the charge-transfer salts derived of $\text{Pd}(\text{dddt})_2$ donor have very similar crystal structure consisting of the stacks of $\text{Pd}(\text{dddt})_2$ dimer units (dimerized stacks). The $\text{Pd}(\text{dddt})_2$ moieties inside the dimer strongly interact mostly due to $\text{Pd}\cdots\text{Pd}$ bonds. The interaction between dimers inside the stacks is weak, while the “side-by-side” interactions via short $\text{S}\cdots\text{S}$ contacts between the dimers in neighboring stacks are stronger. The stacks of $\text{Pd}(\text{dddt})_2$ dimers form conducting layers, which alternate with the insulating anion layers. The $[\text{Pd}(\text{dddt})_2]_2\text{AuBr}_2$ and $[\text{Pd}(\text{dddt})_2]_2\text{SbF}_6$ crystals are isostructural.^{23,24} The unit cell of $[\text{Pd}(\text{dddt})_2]_2\text{AuBr}_2$ crystals is triclinic, space group $P\bar{1}$, with $a=6.498\ \text{Å}$, $b=8.443\ \text{Å}$, $c=15.799\ \text{Å}$, $\alpha=82.07^\circ$, $\beta=83.35^\circ$, $\gamma=67.82^\circ$, $V=793.0\ \text{Å}^3$, $Z=1$; and the interatomic $\text{Pd}\cdots\text{Pd}$ distance inside $\text{Pd}(\text{dddt})_2$ dimer equals to $3.043(0)\ \text{Å}$,²³ The $[\text{Pd}(\text{dddt})_2]_2\text{SbF}_6$ crystals have the following unit-cell parameters: $a=6.498\ \text{Å}$, $b=8.374\ \text{Å}$, $c=16.238\ \text{Å}$, $\alpha=86.81^\circ$, $\beta=87.30^\circ$, $\gamma=68.48^\circ$, $V=820.4\ \text{Å}^3$, space group $P\bar{1}$, $Z=1$; and the intradimer $\text{Pd}\cdots\text{Pd}$ distance equals to $3.034(1)\ \text{Å}$.²⁴ Due to bad crystal quality the crystallographic studies of $[\text{Pd}(\text{dddt})_2]_2\text{TeCl}_x$ ($x=5$ or 6) have not been done but we expect that the structure is very similar. It is supposed that in $[\text{Pd}(\text{dddt})_2]_2\text{TeCl}_x$ salt the anions can be present as two-charge TeCl_6^{2-} or one-charge TeCl_5^- anions,⁹ which gives rise to a disorder in the anion layers and the existence of $\text{Pd}(\text{dddt})_2$ dimers with different charge density.

II. EXPERIMENT

The $\text{Pd}(\text{dddt})_2$ salts were obtained by electrochemical oxidation of a neutral $\text{Pd}(\text{dddt})_2$ complex in nitrobenzene on a Pt anode under constant current $\sim 1\ \mu\text{A}$ at 24.5°C . Typical dimensions of the crystals in the form of elongated plates were about $1\times 0.2\times 0.01\ \text{mm}^3$.

Polarized reflectance spectra were measured from the best-developed crystal face, that is parallel to the conducting $\text{Pd}(\text{dddt})_2$ layers. Infrared measurements from 650 to $6500\ \text{cm}^{-1}$ were carried out on a Fourier transform infrared (FT-IR) Perkin-Elmer 1725X spectrometer equipped with a suitable FT-IR microscope. The incoming IR beam was polarized with a gold wire grid deposited on AgBr substrate. A home made microreflectometer was used to measure the spectra within the frequency region 9000 to $40\ 000\ \text{cm}^{-1}$,

using the Glan-Thompson prism as a polarizer. Between the available $[\text{Pd}(\text{dddt})_2]_2\text{AuBr}_2$ crystals it was possible to find samples thin enough to perform the polarized transmission measurements. The polarized reflectance or transmission experiments were performed in two polarizations: with the electrical vector of polarized light parallel E_{\parallel} and perpendicular E_{\perp} to the $\text{Pd}(\text{dddt})_2$ stacking axis. To study the electronic bands in more detail, we measured also the absorption spectra (from 400 to $40\ 000\ \text{cm}^{-1}$) of finely powdered crystals dispersed in KBr pellets. All the measurements were performed at room temperature.

The frequency dependent optical conductivity and the real part of the dielectric function were obtained by Kramers-Kronig analysis of the reflectance data. The low-frequency data were extrapolated to zero frequency assuming a constant value. For $[\text{Pd}(\text{dddt})_2]_2\text{SbF}_6$ and $[\text{Pd}(\text{dddt})_2]_2\text{AuBr}_2$ above $40\ 000\ \text{cm}^{-1}$ the reflectance data were extended as $R\approx\omega^{-2}$. For $[\text{Pd}(\text{dddt})_2]_2\text{TeCl}_x$ above $6500\ \text{cm}^{-1}$ the spectra were extrapolated on the basis of the data for $[\text{Pd}(\text{dddt})_2]_2\text{SbF}_6$ and above $40\ 000\ \text{cm}^{-1}$ as $R\approx\omega^{-2}$.

Moreover, we studied the Fourier transform near-infrared (FT-NIR) Raman scattering for $[\text{Pd}(\text{dddt})_2]_2\text{TeCl}_x$ powders at the exciting wavelength of $1064\ \text{nm}$ ($1.17\ \text{eV}$) by using a FT-IR Bruker IFS 66 equipped with a FRA 106 Bruker attachment for FT-Raman spectroscopy.

III. RESULTS

The room-temperature reflectance spectra over the entire measured spectral range for the electrical vector of polarized light parallel E_{\parallel} and perpendicular E_{\perp} to the stacking axis are shown in Fig. 2 and Fig. 3, respectively. For $[\text{Pd}(\text{dddt})_2]_2\text{AuBr}_2$ and $[\text{Pd}(\text{dddt})_2]_2\text{SbF}_6$ the experimental data are missing between 6500 and $9000\ \text{cm}^{-1}$, whereas the spectra of $[\text{Pd}(\text{dddt})_2]_2\text{TeCl}_x$ have been only measured in the frequency range 650 to $6500\ \text{cm}^{-1}$. For polarization E_{\parallel} the reflectance spectra of $[\text{Pd}(\text{dddt})_2]_2\text{AuBr}_2$ and $[\text{Pd}(\text{dddt})_2]_2\text{SbF}_6$ salts are similar: in the low-frequency region some narrow peaks, typical for molecular vibrations, and at higher frequencies some electronic features are observed, whereas for polarization E_{\perp} the vibrational features are not found. Analogous behavior shows the reflectance of $[\text{Pd}(\text{dddt})_2]_2\text{TeCl}_x$ crystal within the measured frequency range. The polarized absorption spectra of $[\text{Pd}(\text{dddt})_2]_2\text{AuBr}_2$ crystal for both polarizations are shown in Fig. 4.

The optical conductivity spectra derived by Kramers-Kronig transformation for polarization E_{\parallel} and E_{\perp} are shown in Figs. 5, 6, and 7. The conductivity spectrum of $[\text{Pd}(\text{dddt})_2]_2\text{TeCl}_x$ crystal for polarization E_{\parallel} , and the spectra of both $[\text{Pd}(\text{dddt})_2]_2\text{AuBr}_2$ and $[\text{Pd}(\text{dddt})_2]_2\text{SbF}_6$ crystals exhibit semiconductorlike behavior for both polarizations, while the spectrum of $[\text{Pd}(\text{dddt})_2]_2\text{TeCl}_x$ crystal for E_{\perp} reminds the spectra of metallic-like materials. The real parts of the dielectric function derived by Kramers-Kronig analysis of the reflectance spectra are shown in Figs. 8 and 9.

At low frequency, the conductivity spectra for polarization E_{\parallel} show vibrational features being mostly the consequence of interactions between the charge-transfer transition and the a_g phonon modes of $\text{Pd}(\text{dddt})_2$ molecule (Fig. 7). The IR bands, together with the proposed assignment are

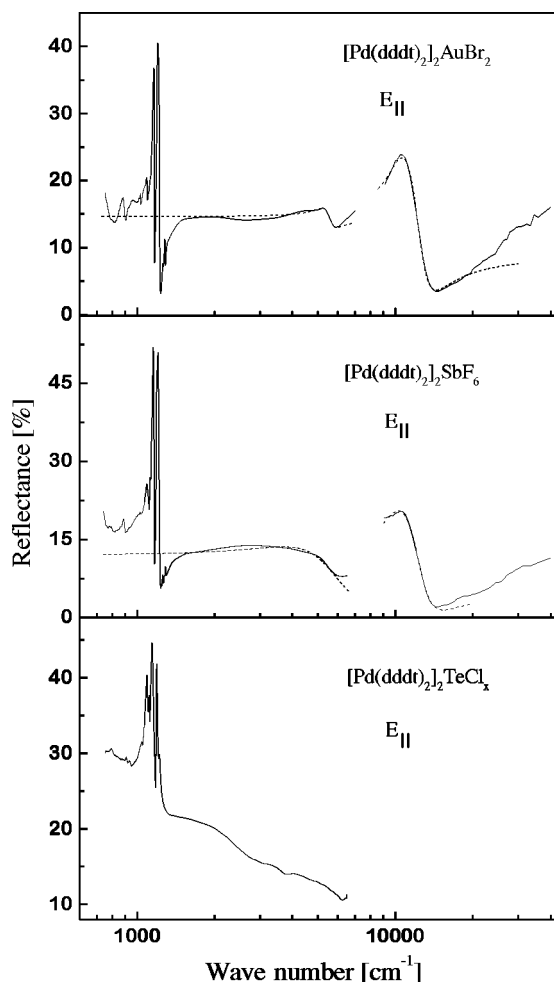


FIG. 2. Polarized reflectance spectra of $[\text{Pd}(\text{ddd})_2]_2\text{AuBr}_2$, $[\text{Pd}(\text{ddd})_2]_2\text{SbF}_6$, and $[\text{Pd}(\text{ddd})_2]_2\text{TeCl}_x$ crystals at room temperature for polarization of the electrical vector of the incident light parallel to the $\text{Pd}(\text{ddd})_2$ stacking axis (note the logarithmic frequency scale). Dotted lines show the Drude-Lorentz fits.

listed in Table I. In Ref. 26 the Raman spectra of single crystals were measured (excitation $\lambda = 6328 \text{ \AA}$) and the following lines related to $\text{Pd}(\text{ddd})_2$ vibrations of a_g symmetry were detected: for $[\text{Pd}(\text{ddd})_2]_2\text{AuBr}_2$ at 1306 cm^{-1} (C=C), 913 and 877 cm^{-1} (C-S), 379 cm^{-1} (Pd-S); and for $[\text{Pd}(\text{ddd})_2]_2\text{SbF}_6$ at 1309 cm^{-1} (C=C), 914 and 875 cm^{-1} (C-S), 379 cm^{-1} (Pd-S). The vibrational peaks for E_{\parallel} are dominated by the two strong bands at about 1190 and 1150 cm^{-1} , which we relate to the coupling of the C=C vibrations of $\text{Pd}(\text{ddd})_2$ with the charge transfer. The presence of such doublet is a characteristic feature of the IR spectra of $M(\text{ddd})_2$ salts: for example, it was previously observed in the spectra of $[\text{Pt}(\text{ddd})_2]_2\text{IBr}_2$ at about 1200 and 1150 cm^{-1} Ref. 19 and the spectra of $[\text{Ni}(\text{ddd})_2]_3(\text{HSO}_4)_2$ at about 1250 and 1160 cm^{-1} .^{20,21} The weaker band situated at about 1100 cm^{-1} in the studied $\text{Pd}(\text{ddd})_2$ crystals was also found in the spectra of $[\text{Pt}(\text{ddd})_2]_2\text{IBr}_2$ and $[\text{Ni}(\text{ddd})_2]_3(\text{HSO}_4)_2$ crystals at about 1080 cm^{-1} (Ref. 19) and 1120 cm^{-1} ,²⁰ respectively, and we attribute it also to the C=C vibrations of $\text{Pd}(\text{ddd})_2$ (see the discussion in Sec. IV D). It should be also noted that in the spectrum of $[\text{Pd}(\text{ddd})_2]_2\text{TeCl}_x$ crystal the band at about 1100 cm^{-1} is much stronger than the analogous band in the

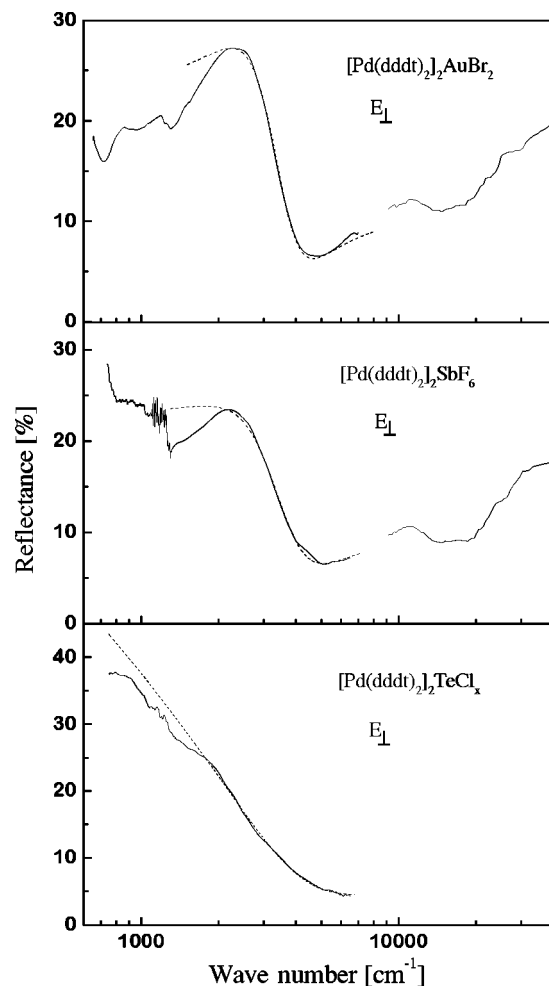


FIG. 3. Polarized reflectance spectra of $[\text{Pd}(\text{ddd})_2]_2\text{AuBr}_2$, $[\text{Pd}(\text{ddd})_2]_2\text{SbF}_6$, and $[\text{Pd}(\text{ddd})_2]_2\text{TeCl}_x$ crystals at room temperature for polarization of the electrical vector of the incident light perpendicular to the $\text{Pd}(\text{ddd})_2$ stacking axis (note the logarithmic frequency scale). Dotted lines show the Drude-Lorentz or Drude in the case of $[\text{Pd}(\text{ddd})_2]_2\text{TeCl}_x$ fits.

spectra of $[\text{Pd}(\text{ddd})_2]_2\text{AuBr}_2$ and $[\text{Pd}(\text{ddd})_2]_2\text{SbF}_6$ crystals. On closer examination of the spectra of our crystals some additional weaker vibrational bands can be also distinguished (Table I).

For polarization perpendicular to the $\text{Pd}(\text{ddd})_2$ stacks (E_{\perp}) the vibrational bands due to the electron-phonon coupling are not observed. This is in agreement with the common behavior of IR spectra of BEDT-TTF salts measured in the direction of strong ‘‘side-by-side’’ $\text{S}\cdots\text{S}$ interactions.²⁵ Instead, we observe some very weak peaks which may be attributed to the IR active in-plane modes of $\text{Pd}(\text{ddd})_2$ molecule (Figs. 4 and 6).

For polarization E_{\parallel} the vibrational bands are partially superimposed on a broad electronic absorption with the maximum at about 5300 cm^{-1} (Figs. 5 and 7). This electronic feature is a superposition of two bands at least. As seen in Figs. 4 and 5 (upper panel), in the spectrum of $[\text{Pd}(\text{ddd})_2]_2\text{AuBr}_2$ crystal one can distinguish a stronger band centered at 5350 cm^{-1} and a weaker one centered at 2650 cm^{-1} . Similar conclusion results from the analysis of the conductivity spectrum of $[\text{Pd}(\text{ddd})_2]_2\text{TeCl}_x$ crystal, nevertheless, for $[\text{Pd}(\text{ddd})_2]_2\text{SbF}_6$ the existence of two low-

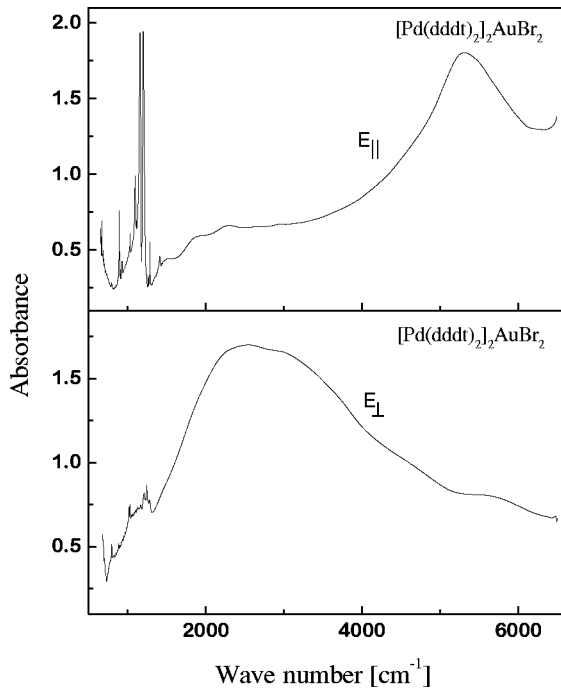


FIG. 4. Polarized infrared absorption spectra of $[\text{Pd}(\text{ddd})_2]_2\text{AuBr}_2$ crystal for polarization parallel E_{\parallel} and perpendicular E_{\perp} to the stacking axis.

frequency electronic bands is not so clear (Fig. 5). For polarization E_{\perp} the conductivity spectra are also dominated by a strong electronic absorption but it is centered at lower frequency: about 2300 cm^{-1} for $[\text{Pd}(\text{ddd})_2]_2\text{AuBr}_2$, about 2600 cm^{-1} for $[\text{Pd}(\text{ddd})_2]_2\text{SbF}_6$ and about 1800 cm^{-1} for $[\text{Pd}(\text{ddd})_2]_2\text{TeCl}_x$ (Fig. 6). The electronic absorption for E_{\perp} is supposed to be a superposition of analogous bands as those observed for polarization E_{\parallel} but the oscillator strength distribution is different. For example, for $[\text{Pd}(\text{ddd})_2]_2\text{AuBr}_2$ the intensity of band at 2650 cm^{-1} is larger than that of the band at 5350 cm^{-1} (Fig. 4).

At higher frequencies the optical conductivity spectra show another electronic band at about $10\,600\text{ cm}^{-1}$ (Figs. 5 and 6). To study the electronic features in more detail we measured also the absorption spectra of $[\text{Pd}(\text{ddd})_2]_2\text{TeCl}_x$ salt dispersed in KBr pellet (Fig. 10). We observed a strong band at about 9300 cm^{-1} and three higher-frequency bands situated at about $14\,600$, $26\,800$, and $37\,000\text{ cm}^{-1}$. The main vibrational bands are present at the frequencies: 1405 (*m*), 1346 (*w*), 1300 (*m*), 1285 (*m*), 1249 (*s*), 1230 (*s*), 1191 (*m*), 1163 (*m*), 1155 (*m*), 1112 (*w*), 1090 (*w*), 921 (*w*), and 893 cm^{-1} (*w*). The strong bands at 1249 and 1230 cm^{-1} dominate the vibrational spectrum of powdered salt and should be assigned to the in plane IR active vibrations of $\text{Pd}(\text{ddd})_2$ (probably C=C vibrations of b_{1u} symmetry). Since the planes of $\text{Pd}(\text{ddd})_2$ are nearly perpendicular to the best-developed crystal face, such strong bands are not observed in the reflectance spectrum. The bands 1191 and 1155 cm^{-1} as well as 1112 and 1090 cm^{-1} we attribute to the C=C vibrations of $\text{Pd}(\text{ddd})_2$ coupled with electrons. The positions of C=C bands in KBr spectrum differ from those found in reflectance data (Table I). This difference can be related to the interaction with KBr matrix. In addition, a degeneration of the sample due to the preparation of the KBr

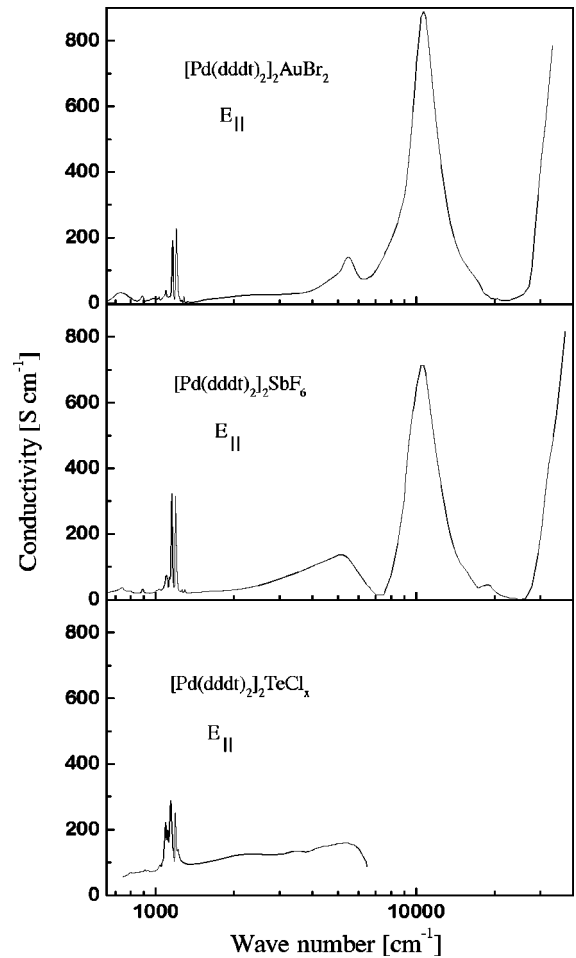


FIG. 5. Optical conductivity of the studied crystals as obtained by Kramers-Kronig analysis of the reflectance data parallel to the $\text{Pd}(\text{ddd})_2$ stacking axis E_{\parallel} .

pellet surely enhances the disorder existing in $[\text{Pd}(\text{ddd})_2]_2\text{TeCl}_x$ crystals.

We investigated also FT-NIR Raman scattering of powdered $[\text{Pd}(\text{ddd})_2]_2\text{TeCl}_x$ crystals in KBr pellet and the following peaks were found: 1347 (*m*), 1264 (*w*), 1228 (*m*), 1164 (*w*), 897 (*s*), 886 (*s*), 833 (*w*), 759 (*w*), 519 (*w*), 453 (*m*), and 380 cm^{-1} (*s*). We assign the bands at 1347 , 1264 , and 1228 cm^{-1} to the Raman active totally symmetric C=C vibrations of various $\text{Pd}(\text{ddd})_2$ ions (a_g modes), i.e., $[\text{Pd}(\text{ddd})_2]^0$, $[\text{Pd}(\text{ddd})_2]^+$ and $[\text{Pd}(\text{ddd})_2]^{2+}$, respectively. The disorder existing in $[\text{Pd}(\text{ddd})_2]_2\text{TeCl}_x$ salt is considerably increased by powdering of the sample and leads to the charge localization; as a result different $\text{Pd}(\text{ddd})_2$ ions are created. The doublet 897 and 886 cm^{-1} is due to C-S vibrations and the band at 380 cm^{-1} corresponds to Pd-S stretching. The obtained Raman frequencies can be compared with the single-crystal data reported in Ref. 26: for neutral $[\text{Pd}(\text{ddd})_2]^0$ the C=C vibration was observed at 1350 cm^{-1} , the C-S vibration at 896 cm^{-1} , and Pd-S vibration at 378 cm^{-1} .

IV. DISCUSSION

A. Electronic features

The low-frequency electronic absorption, i.e., with maximum at about 5300 cm^{-1} for polarization E_{\parallel} and at lower

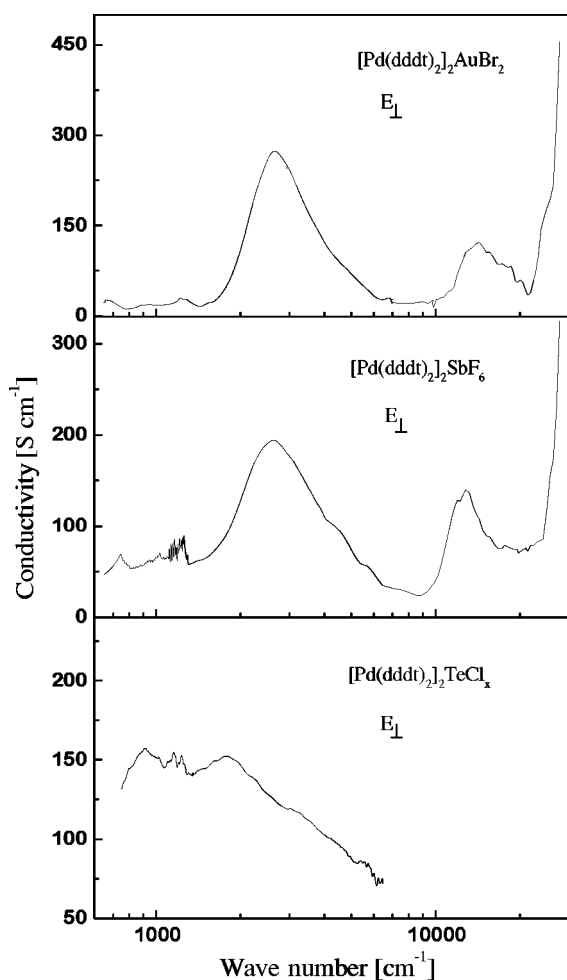


FIG. 6. Optical conductivity of the studied crystals as obtained by Kramers-Kronig analysis of the reflectance data perpendicular to the $\text{Pd}(\text{ddd})_2$ stacking axis E_{\perp} .

energies, i.e., below 3000 cm^{-1} for polarization E_{\perp} , should be related to the charge transfer process: $\text{Pd}(\text{ddd})_2^+ + \text{Pd}(\text{ddd})_2^0 = \text{Pd}(\text{ddd})_2^0 + \text{Pd}(\text{ddd})_2^+$ (CT_2 band).^{20,27} For polarization parallel to the stacking axis (E_{\parallel}) this electronic absorption can be a superposition of the intra- and interdimer transitions inside the $\text{Pd}(\text{ddd})_2$ stacks but we assume that it is mainly due to the intradimer transitions, since the interactions between dimers are much weaker. For polarization E_{\perp} these bands correspond to the CT_2 charge-transfer excitation taking place between the neighboring $\text{Pd}(\text{ddd})_2$ stacks (side-by-side interaction between molecules). Note that, due to the strong $S \dots S$ interactions between stacks, the energies of CT_2 bands for E_{\perp} are lower than the suitable energies for polarization E_{\parallel} . On closer examination of broad CT_2 bands it results that they are a superposition of two electronic features at least, what should be related to the existence of different charge-transfer transitions. Because of the small HOMO-LUMO splitting in the $\text{Pd}(\text{ddd})_2$ molecule, different CT_2 charge-transfer transitions inside the $\text{Pd}(\text{ddd})_2$ dimers are possible. For polarization perpendicular to the stacks (E_{\perp}) the structure of CT_2 band can be explained in the same way, however, due to different overlap of molecular orbitals in this direction, the oscillator strength distribution between the two peaks is different.

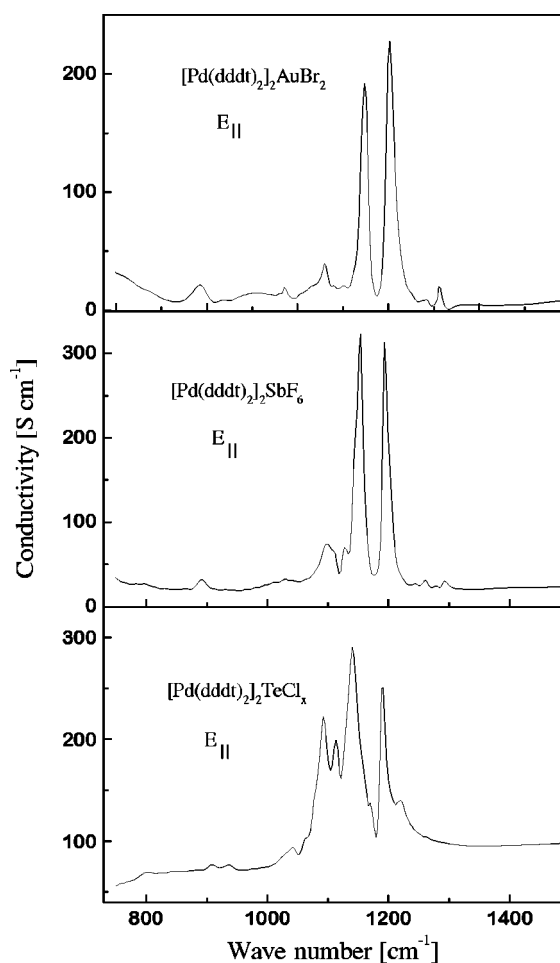


FIG. 7. Optical conductivity within the region of vibrational bands (polarization E_{\parallel}).

The electronic band at about 10600 cm^{-1} observed for both polarizations can be attributed to the charge-transfer transition: $\text{Pd}(\text{ddd})_2^+ + \text{Pd}(\text{ddd})_2^+ = \text{Pd}(\text{ddd})_2^0 + \text{Pd}(\text{ddd})_2^{2+}$ (CT_1 band).^{20,27} The position of this band can be approximately described by the value of the effective Coulomb interaction, which is proportional to $(U-V)$, the Hubbard parameters for on-site and nearest-neighbor Coulomb repulsion energies, respectively. Assuming that V is small the position of this band is a measure of the on-site Coulomb repulsion between charges on the same $\text{Pd}(\text{ddd})_2$ molecule. The value $U = 10600 \text{ cm}^{-1}$ is comparable to those found for $\text{Pt}(\text{ddd})_2$ (Ref. 19) and $\text{Ni}(\text{ddd})_2$ (Refs. 20 and 21) salts, as well as BEDT-TTF salts,²⁰ but it is considerably larger than those found for $\text{Ni}(\text{dmit})_2$ salts (5560 and 8000 cm^{-1}).²⁸ The high-frequency electronic features at about 14600 , 26800 , and 37000 cm^{-1} are related to intramolecular excitations of $\text{Pd}(\text{ddd})_2$.

B. Electronic structure

As seen in Fig. 5, a maximum of optical conductivity at about 5200 cm^{-1} is observed for the stacking axis polarization E_{\parallel} . Such conductivity maximum is usually related to the presence of a gap in the electronic excitation spectrum. Analogous behavior is found in the perpendicular polarization E_{\perp} for $[\text{Pd}(\text{ddd})_2]_2\text{AuBr}_2$ and $[\text{Pd}(\text{ddd})_2]_2\text{SbF}_6$ salts, whereas it is different for $[\text{Pd}(\text{ddd})_2]_2\text{TeCl}_x$ crystal (Fig. 6).

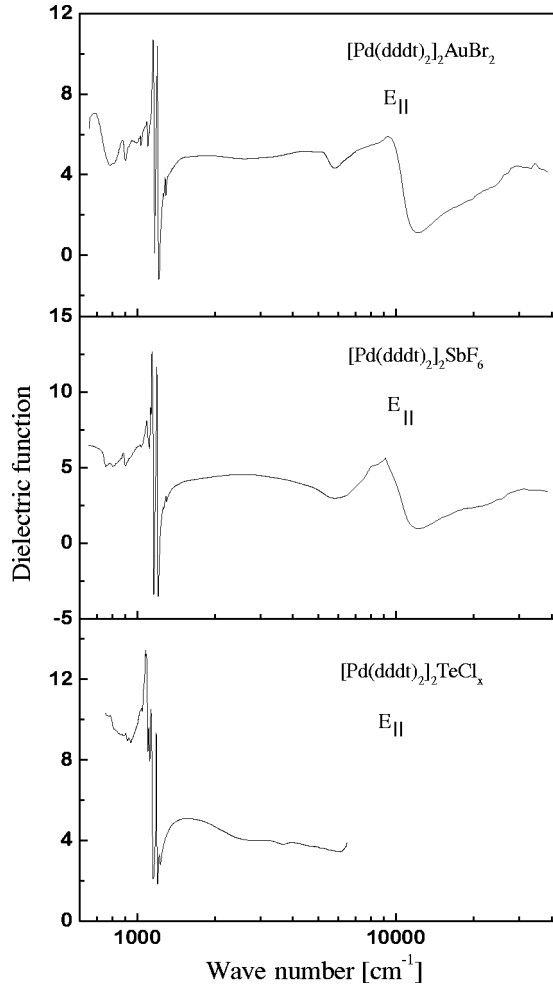


FIG. 8. Real part of the dielectric function of the studied crystals as obtained by Kramers-Kronig analysis for light polarized parallel to the $\text{Pd}(\text{ddd})_2$ stacking axis E_{\parallel} .

The low-frequency electronic dispersion of crystals exhibiting semiconducting properties is usually analyzed by a Drude-Lorentz dielectric function. In the studied $\text{Pd}(\text{ddd})_2$ crystals this absorption is expected to be a superposition of two electronic contributions. Consequently, the experimental reflectance should be analyzed using a sum of two Lorentz oscillators but such procedure is not reliable in the case of so strongly overlapping bands. For this reason we have fitted the experimental data by a single Drude-Lorentz function

$$\varepsilon(\omega) = \varepsilon_{\infty} + \frac{\omega_p^2}{\omega_0^2 - \omega^2 - i\omega\Gamma}, \quad (1)$$

where ω_p is the plasma frequency, ω_0 is the center frequency, Γ is the scattering rate, and ε_{∞} represents all higher-frequency contributions to the dielectric function.

The fits were made to the data between 1800 and 6500 cm^{-1} and the best results are listed in Table II. The distinct deviations from Drude-Lorentz behavior observed at lower frequencies are due to the short-range electron-electron and electron-phonon interactions, nevertheless, it is assumed that the plasmon frequency is insensitive to the detailed nature of these interactions.²⁹ For polarization E_{\parallel} an additional Lorentz term was introduced in the fitting procedure

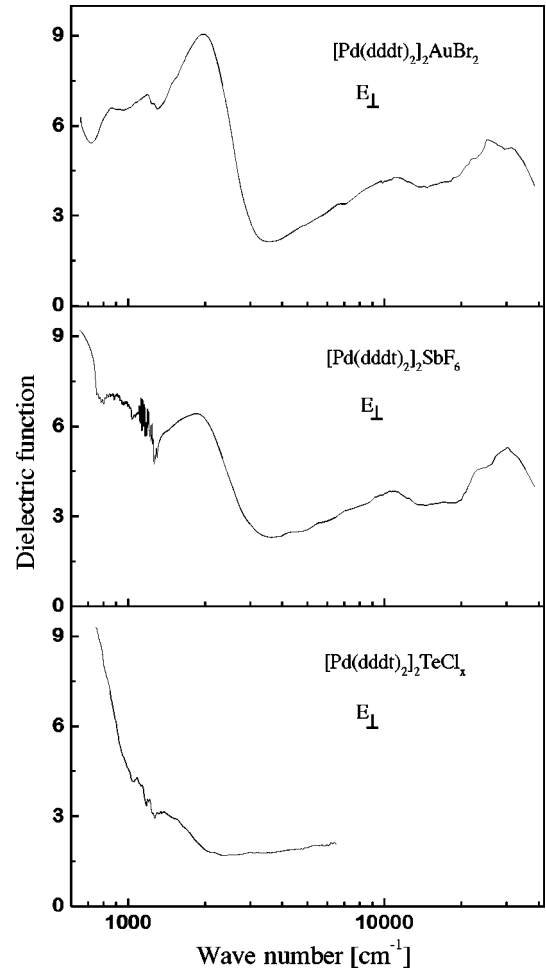


FIG. 9. Real part of the dielectric function of the studied crystals as obtained by Kramers-Kronig analysis for light polarized perpendicular to the $\text{Pd}(\text{ddd})_2$ stacking axis E_{\perp} .

to describe the structure around 10 600 cm^{-1} (see Fig. 2). The application of function (1) to the reflectance data of $[\text{Pd}(\text{ddd})_2]_2\text{AuBr}_2$ for E_{\parallel} is not very satisfactory (Fig. 2), probably due to the two-banded structure, but a better result is obtained for polarization E_{\perp} (Fig. 3). In the analogous way, acceptable fits were also obtained for $[\text{Pd}(\text{ddd})_2]_2\text{SbF}_6$ in both polarizations.

On the other hand, the reflectance of $[\text{Pd}(\text{ddd})_2]_2\text{TeCl}_x$ crystal for polarization E_{\perp} was fitted with a simple Drude dielectric function

$$\varepsilon(\omega) = \varepsilon_{\infty} - \frac{\omega_p^2}{\omega(\omega + i\Gamma)}, \quad (2)$$

where ω_p , ε_{∞} and Γ have the same meaning as in Eq. (1). The fit was made to the data between 1800 and 6500 cm^{-1} , the best fit parameters are $\varepsilon_{\infty} = 2.9$, $\omega_p = 7200 \text{ cm}^{-1}$, $\Gamma = 5650 \text{ cm}^{-1}$, and the fit quality is shown in Fig. 3 (bottom panel).

The fit results allow us to determine the band-structure parameters for $[\text{Pd}(\text{ddd})_2]_2\text{AuBr}_2$ and $[\text{Pd}(\text{ddd})_2]_2\text{SbF}_6$ crystals. The effective mass of carriers m^* is related to the plasma frequency by the equation

TABLE I. Frequencies (cm^{-1}) and assignments of vibrational bands for polarization E_{\parallel} (see text).

$[\text{Pd}(\text{ddd})_2]_2\text{AuBr}_2$	$[\text{Pd}(\text{ddd})_2]_2\text{SbF}_6$	$[\text{Pd}(\text{ddd})_2]_2\text{TeCl}_x$	Assignment
1283w	1292w	1219w	
	1261w		
1196s	1193s	1190s	$a_g(\text{C}=\text{C})$
		1170w	
1154s	1154s	1140s	$a_g(\text{C}=\text{C})$
1124m	1128m	1113s	$a_g(\text{C}=\text{C})$
	1109w		
1094m	1098m	1092s	$a_g(\text{C}=\text{C})$
924m		936m	$a_g(\text{C}-\text{S})$
913m	892m	908m	$a_g(\text{C}-\text{S})$

$$\omega_p^2 = \frac{4\pi n e^2}{m^*}, \quad (3)$$

where n is the concentration of carriers, e is the electron charge and the values of ω_p are derived from the Drude-Lorentz model.²⁹ The concentration of holes was found from the structural data^{23,24} to be $n = 1.261 \times 10^{21} \text{ cm}^{-3}$ for $[\text{Pd}(\text{ddd})_2]_2\text{AuBr}_2$ and $n = 1.219 \times 10^{21} \text{ cm}^{-3}$ for $[\text{Pd}(\text{ddd})_2]_2\text{SbF}_6$ [assuming one positive charge per two $\text{Pd}(\text{ddd})_2$ molecules]. For $[\text{Pd}(\text{ddd})_2]_2\text{AuBr}_2$ we found $m^*/m_0 = 1.05$ and $m^*/m_0 = 1.02$ for the direction parallel and perpendicular to the stacking axis, respectively. In the case of $[\text{Pd}(\text{ddd})_2]_2\text{SbF}_6$ crystal we obtained the value $m^*/m_0 = 1.01$ for both directions. The effective masses of holes are almost the same in the two main directions and they are nearly equal to the mass of free carriers. Since the studied compounds possess ‘‘two-band’’ electronic structure, it should be emphasized that the estimated effective masses m^* are mean values over LUMO and HOMO holes.

The description of electronic structure may be continued by applying a simplified tight-binding band-structure model proposed by Jacobsen *et al.*³⁰ to estimate the anisotropy in the conducting layer. In this model it is assumed that the IR response near the plasmon frequency is insensitive to the detailed nature of the short-range electron-electron and electron-phonon interactions, which yield deviations in the low-frequency range. If transfer integrals parallel t_{\parallel} and perpendicular t_{\perp} are introduced, the band structure can be represented as

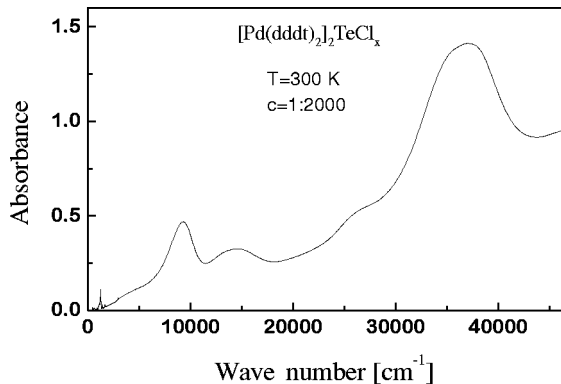


FIG. 10. Electronic absorption spectrum of $[\text{Pd}(\text{ddd})_2]_2\text{TeCl}_x$ powders dispersed in KBr pellet (weight concentration 1:2000)

$$E(k_{\parallel}, k_{\perp}) = -2t_{\parallel} \cos(k_{\parallel} d_{\parallel}) - 2t_{\perp} \cos(k_{\perp} d_{\perp}), \quad (4)$$

where d_{\parallel} is the mean molecular repeat distance along the stacks and d_{\perp} the repeat distance perpendicular to the stacks. The transfer integral t_{\parallel} is an average value along the stack, and t_{\perp} is a weighted average of several interchain transfer integrals in the correct band structure. Subsequently, we can estimate the optical anisotropy factor $(\omega_{p\parallel}/\omega_{p\perp})(d_{\perp}/d_{\parallel})$ which equals to 1.65 for $[\text{Pd}(\text{ddd})_2]_2\text{AuBr}_2$ (molecular repeat distances $d_{\parallel} = 3.89$ and $d_{\perp} = 6.00 \text{ \AA}$) and it has the value 1.90 for $[\text{Pd}(\text{ddd})_2]_2\text{SbF}_6$ (molecular repeat distances $d_{\parallel} = 3.89$ and $d_{\perp} = 6.04 \text{ \AA}$). For $[\text{Pd}(\text{ddd})_2]_2\text{AuBr}_2$ the respective value t_{\perp}/t_{\parallel} estimated on basis of the numerical results of Ref. 30 is 0.54, and $t_{\perp} = 0.10$ and $t_{\parallel} = 0.05$ eV. Analogously for $[\text{Pd}(\text{ddd})_2]_2\text{SbF}_6$ we obtained $t_{\perp}/t_{\parallel} = 0.48$, $t_{\perp} = 0.14$, and $t_{\parallel} = 0.07$ eV (Table II). From these data it results that in both salts the bands are nearly isotropic and the expected Fermi surface is closed.

C. Sum rule

When one-electron model is applicable, the electronic structure parameters can be achieved by the standard partial sum rule³¹

$$I_{\sigma}(\omega) = \frac{2}{\epsilon_0 \pi} \int_0^{\omega} \sigma(\omega') d\omega', \quad (5)$$

$$\left[\frac{m_0}{m^*} \right] N_{eff}(\omega) = \frac{m_0 \epsilon_0}{64 N_c e^2} I_{\sigma}(\omega), \quad (6)$$

where m^* is the effective mass of the carriers, m_0 is the electronic mass, N_c is the number of conduction electrons per unit volume, and in the case of the saturation limit $I_{\sigma}(\omega)$ is ω_p^2 . Deviations from such behavior will lead to a saturation limit of $I_{\sigma}(\omega)$ being lower than ω_p^2 .

In Fig. 11 we show $I_{\sigma}(\omega)$ and ω_p^2 for $[\text{Pd}(\text{ddd})_2]_2\text{AuBr}_2$ crystal (upper panel) and $[\text{Pd}(\text{ddd})_2]_2\text{SbF}_6$ crystal (bottom panel) estimated from the optical conductivity parallel E_{\parallel} and perpendicular E_{\perp} to the stacking direction. In order to calculate the values of the integral $I_{\sigma}(\omega)$, the optical conductivity was extrapolated to $\omega \rightarrow 0$ using a constant value. While only a small deviation from the sum rule (5) is found for polarization E_{\perp} , the deviation for polarization E_{\parallel} is higher, especially in the case of $[\text{Pd}(\text{ddd})_2]_2\text{SbF}_6$. This de-

TABLE II. Transport parameters obtained from the analysis of the reflectance spectra by the Drude-Lorentz model.

Salt	Polarization	ϵ_∞	ω_0 (cm ⁻¹)	ω_p (cm ⁻¹)	Γ (cm ⁻¹)	m^*/m_0	t (eV)	$4t$ (eV)
[Pd(dddtd) ₂] ₂ AuBr ₂	E_{\parallel}	3.3	5510	5700	2240	1.05	0.05	0.20
	E_{\perp}	3.9	2620	5320	1890	1.02	0.10	0.40
[Pd(dddtd) ₂] ₂ SbF ₆	E_{\parallel}	2.4	4930	6730	4150	1.01	0.07	0.28
	E_{\perp}	3.6	2660	5490	2680	1.01	0.14	0.56

viation may be due to electron–molecular vibration (EMV) coupling as well as short-range electron–electron interactions. Since the EMV-coupling phenomena are only found in the direction parallel to the stacking axis E_{\parallel} and the deviations from Eq. (5) dominate in this direction, we suggest that the EMV coupling contributes to a high extent to this deviation. Nevertheless, a contribution of the electron–electron interactions can be also considerable.

In the stacking direction E_{\parallel} , the value of $I_{\sigma}(\omega)$ at first rises in the low-frequency region, begins to level off at a value near $1.01 \times 10^{30} \text{ s}^{-2}$ and $0.64 \times 10^{30} \text{ s}^{-2}$ in the near infrared for [Pd(dddtd)₂]₂AuBr₂ and [Pd(dddtd)₂]₂SbF₆, respectively, and then rises rapidly again above the onset of the high-frequency electronic bands, reaching $5.42 \times 10^{30} \text{ s}^{-2}$ at $21\,900 \text{ cm}^{-1}$ for [Pd(dddtd)₂]₂AuBr₂ and $5.02 \times 10^{30} \text{ s}^{-2}$ at $21\,400 \text{ cm}^{-1}$ for [Pd(dddtd)₂]₂SbF₆. From the plateau values of the integrated oscillation strengths in the near infrared, assuming N_{eff} for [Pd(dddtd)₂]₂AuBr₂ and [Pd(dddtd)₂]₂SbF₆ to be 0.5, we estimate $m^* = 1.00m_0$ and $m^* = 1.56m_0$, respectively.

In the direction perpendicular to the stacking axis E_{\perp} , $I_{\sigma}(\omega)$ rises rapidly in the low-frequency region, begins to

level off at a value near $0.64 \times 10^{30} \text{ s}^{-2}$ and $0.96 \times 10^{30} \text{ s}^{-2}$ in the near infrared for [Pd(dddtd)₂]₂AuBr₂ and [Pd(dddtd)₂]₂SbF₆, respectively, and then rises rapidly again above the onset of the high-frequency electronic bands, reaching $1.61 \times 10^{30} \text{ s}^{-2}$ at $21\,700 \text{ cm}^{-1}$ for [Pd(dddtd)₂]₂AuBr₂ and $2.21 \times 10^{30} \text{ s}^{-2}$ at $21\,500 \text{ cm}^{-1}$ for [Pd(dddtd)₂]₂SbF₆. From the plateau values of the integrated oscillation strengths in the near infrared, assuming N_{eff} of [Pd(dddtd)₂]₂AuBr₂ and [Pd(dddtd)₂]₂SbF₆ to be 0.5, we estimate $m^* = 1.56m_0$ and $m^* = 1.02m_0$, respectively. These data and the effective masses calculated from plasma frequency are compared in Table III.

D. Electron-phonon coupling

It is well known that in conducting charge transfer crystals the electrons interact strongly with the totally symmetric vibrations of molecules (so called a_g modes) and strong bands corresponding to this interaction dominate their IR spectra.^{18,27} In organic conductors formed by the TTF derivatives the strongest electron–molecular vibration (EMV)–coupling effect is observed for the C=C stretching vibrations. For example, BEDT-TTF molecule has two C=C vibrations of a_g symmetry: $\nu_2(a_g) = 1551 \text{ cm}^{-1}$ and $\nu_3(a_g) = 1493 \text{ cm}^{-1}$.³² These modes are coupled stretching vibrations of both central and ring C=C bonds and their proximity leads to a strong mixing. In the $M(\text{dddtd})_2$ and $M(\text{dmit})_2$ complexes the central C=C bond is replaced by a metal, therefore, their salts are good systems for investigations of the interactions between electrons and the C=C ring bond vibrations. In Ni(dmit)₂ there is one C=C normal a_g mode at 1408 cm^{-1} .³³ Similarly as $M(\text{dmit})_2$, the $M(\text{dddtd})_2$ complex has one totally symmetric a_g mode attributed to C=C stretching: the Raman scattering experiments have shown that for neutral Pd(dddtd)₂ molecule this mode lies at 1350 cm^{-1} .²⁶

The EMV coupling phenomena in conducting charge-transfer salts were analyzed in terms of various models depending on structure of the molecular stacks. Microscopic theories for regular stacks or stacks consisting of quasi-isolated dimers, trimers, tetramers or n -mers have been developed.³⁴ In the studied crystals the conducting layers consist of Pd(dddtd)₂ dimers, therefore, the model of isolated dimers with one unpaired electron seems to be the most appropriate. However, as discussed above, the vibrational C=C mode of Pd(dddtd)₂ is split into a doublet, as was also found in the IR spectra of Pt(dddtd)₂ and Ni(dddtd)₂ salts.^{19,20} The origin of the doublet structure should be explained by the proposed model of electron-phonon coupling.

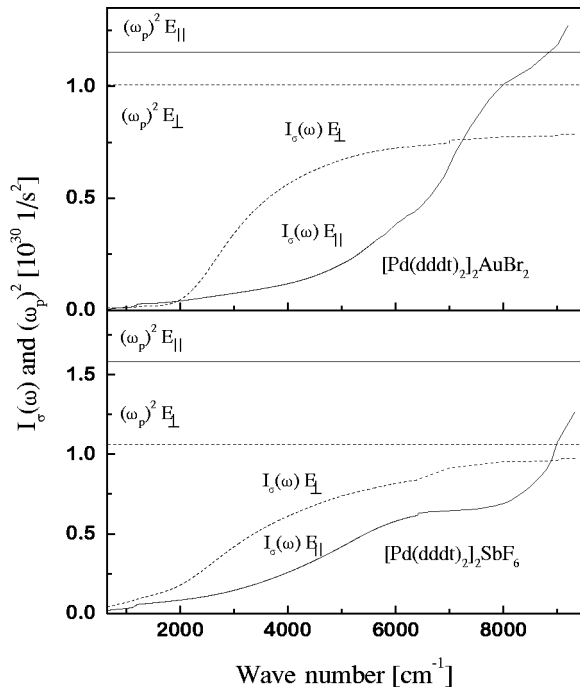


FIG. 11. Sum rule calculations based on the optical conductivity data for [Pd(dddtd)₂]₂AuBr₂ (upper panel) and [Pd(dddtd)₂]₂SbF₆ (bottom panel). The straight lines represent the plasma frequencies obtained by fitting of the Drude model to the dispersion of reflectance.

TABLE III. The effective mass of the carriers calculated for $[\text{Pd}(\text{dddt})_2]_2$ for $[\text{Pd}(\text{dddt})_2]_2\text{SbF}_6$ and $[\text{Pd}(\text{dddt})_2]_2\text{AuBr}_2$

The ratio m^*/m_0 calculated	$[\text{Pd}(\text{dddt})_2]_2\text{AuBr}_2$		$[\text{Pd}(\text{dddt})_2]_2\text{SbF}_6$	
	E_{\parallel}	E_{\perp}	E_{\parallel}	E_{\perp}
From sum rule	1.00	1.56	1.56	1.02
From $\omega_p = (4\pi n e^2/m^*)^{1/2}$	1.05	1.02	1.01	1.01

In general, the splitting of a_g phonon modes is attributed to unevenly localized charge distribution between the molecules forming the salt. The frequency of a_g mode depends on the equilibrium charge distribution and coupling of different oscillators with charge-transfer results in a doublet.³⁴ However, such explanation seems to be not appropriate in our case since only one line in the C=C region was found in Raman spectra of $[\text{Pd}(\text{dddt})_2]_2\text{SbF}_6$ and $[\text{Pd}(\text{dddt})_2]_2\text{AuBr}_2$ salts,²⁶ proving thus an uniform distribution of charge density between the $\text{Pd}(\text{dddt})_2$ monomers in dimers. The possibility that splitting is a consequence of the coupling of the a_g mode with intra- and interdimer charge-transfer excitations should be also ignored since the oscillator strength is nearly evenly distributed between the two peaks of the doublet.

We suggest that the a_g mode splitting should be related to the existence of the “two-band” electronic system in the studied materials. The doublet is a consequence of coupling of C=C a_g phonon mode with HOMO and LUMO electrons. As shown above (see, e.g., Fig. 4), one can distinguish at least two CT_2 charge-transfer excitations in the electronic spectra for the polarization parallel to the stacking axis E_{\parallel} . These bands could be related to the charge-transfer transitions of different electrons (HOMO or LUMO) which interact with the a_g phonon mode yielding the doublet structure. However, as mentioned above, in the $[\text{Pd}(\text{dddt})_2]_2\text{TeCl}_x$ crystal there exist molecules with different charge density, i.e., $\text{Pd}(\text{dddt})_2^0$, $\text{Pd}(\text{dddt})_2^{0.5+}$ and $\text{Pd}(\text{dddt})_2^+$. The frequency of the totally symmetric C=C vibration decreases gradually with decreasing the number of valence electrons in the $M(\text{dddt})_2$ complexes.²⁶ Consequently, different doublets in IR spectrum of $[\text{Pd}(\text{dddt})_2]_2\text{TeCl}_x$ could be assigned to $\text{Pd}(\text{dddt})_2$ moieties with different charge. We relate tentatively the doublet at 1190 and 1140 cm^{-1} to the $\text{Pd}(\text{dddt})_2^{0.5+}$ and the weaker doublet at 1113 and 1092 cm^{-1} to $\text{Pd}(\text{dddt})_2^+$ ions. It is to be supposed that in $[\text{Pd}(\text{dddt})_2]_2\text{TeCl}_x$ the concentration of $\text{Pd}(\text{dddt})_2^+$ ions is quite large, therefore, the respective peaks are relatively strong.

In $[\text{Pd}(\text{dddt})_2]_2\text{SbF}_6$ and $[\text{Pd}(\text{dddt})_2]_2\text{AuBr}_2$ salts the average charge residing on $\text{Pd}(\text{dddt})_2$ equals to $+0.5e$ and the vibration of $\text{Pd}(\text{dddt})_2$ molecules with such charge density couple with HOMO and LUMO electrons yielding two peaks at about 1195 and 1154 cm^{-1} (Table I). At lower frequency in the spectra of $[\text{Pd}(\text{dddt})_2]_2\text{SbF}_6$ and $[\text{Pd}(\text{dddt})_2]_2\text{AuBr}_2$ salts we find also two doublets: 1128 and 1098 cm^{-1} , 1124 and 1094 cm^{-1} , respectively. Similarly as in $[\text{Pd}(\text{dddt})_2]_2\text{TeCl}_x$ salt, these doublets could be related to the $\text{Pd}(\text{dddt})_2^+$ ions. However, in these salts the $\text{Pd}(\text{dddt})_2^+$ ions are not so numerous as in $[\text{Pd}(\text{dddt})_2]_2\text{TeCl}_x$, therefore, the respective bands are much weaker.

The EMV coupling phenomena in $[\text{Pd}(\text{dddt})_2]_2\text{AuBr}_2$ and $[\text{Pd}(\text{dddt})_2]_2\text{SbF}_6$ salts have been analyzed in terms of the model of isolated $\text{Pd}(\text{dddt})_2$ dimer. The solution of EMV-coupling problem for an isolated tetracyanoquinodimethane (TCNQ) dimer with one electron per two TCNQ molecules has been given by Rice, Yartsev, and Jacobsen.³⁵ The complex dielectric function is

$$\varepsilon(\omega) = \varepsilon_{\infty} + \frac{4\pi n e^2 d^2 \frac{2t^2}{\omega_{CT}}}{\omega_{CT}^2 [1 - D(\omega)] - \omega^2 - i\omega\Gamma}, \quad (7)$$

where ω_{CT} determines the position of the charge-transfer peak in the absence of vibrational coupling, Γ is an electronic relaxation rate, ε_{∞} is the background dielectric constant, t is the chain-axis transfer integral, d is the spacing between the molecules and $n = N/V$ is the molecular density (N is the number of molecules in the cluster and V is the volume of the system). The function

$$D(\omega) = \sum_{\alpha} \frac{\lambda_{\alpha} \omega_{\alpha}^2}{\omega_{\alpha}^2 - \omega^2 - i\omega\gamma_{\alpha}}, \quad (8)$$

is the phonon propagator. The ω_{α} and γ_{α} refer to the unperturbed resonant frequencies of the totally symmetric vibrational modes and corresponding linewidths, respectively. The λ_{α} are dimensionless coupling constants, related to the electron-molecular vibration (EMV)-coupling constants g_{α} by

$$\lambda_{\alpha} = \frac{8t^2 g_{\alpha}^2}{\omega_{CT}^3 \omega_{\alpha}}. \quad (9)$$

TABLE IV. The calculated a_g mode frequencies and linear electron-molecular vibrational-coupling constants, and the vibronic parameters used in the dimer model fit to $[\text{Pd}(\text{dddt})_2]_2\text{SbF}_6$ and $[\text{Pd}(\text{dddt})_2]_2\text{AuBr}_2$

$[\text{Pd}(\text{dddt})_2]_2\text{AuBr}_2$			$[\text{Pd}(\text{dddt})_2]_2\text{SbF}_6$		
ε_{∞}	3.4		ε_{∞}	2.4	
t (eV)	0.27		t (eV)	0.28	
ω_{CT} (cm^{-1})	5500		ω_{CT} (cm^{-1})	4900	
Γ (cm^{-1})	2240		Γ (cm^{-1})	2700	
2Δ (eV)	0.42		2Δ (eV)	0.24	
ω_{α} (cm^{-1})	g_{α} (cm^{-1})	λ_{α}	ω_{α} (cm^{-1})	g_{α} (cm^{-1})	λ_{α}
1306	961	0.16	1309	831	0.18
1175	161	0.005	1172	144	0.006

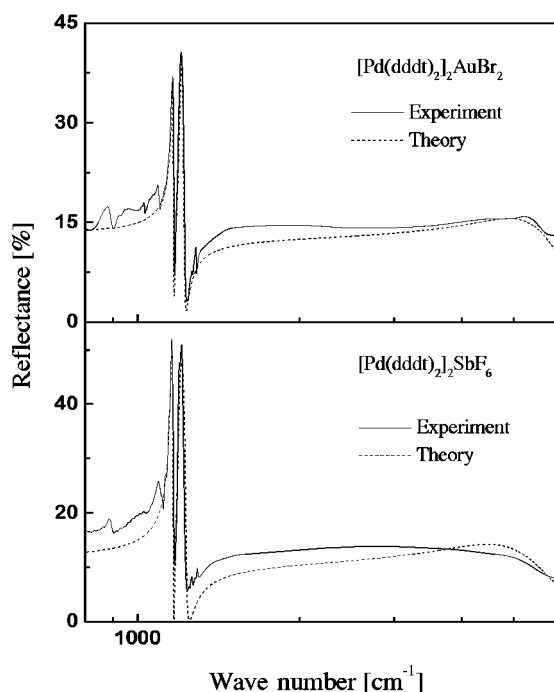


FIG. 12. Fit of the dimer model (dotted line) to the reflectance spectra of $[\text{Pd}(\text{ddd})_2]_2\text{SbF}_6$ and $[\text{Pd}(\text{ddd})_2]_2\text{AuBr}_2$ crystals for polarization parallel to the stacking axis E_{\parallel} (solid line).

We have analyzed our infrared results within the framework of this isolated dimer model taking into account the available structural data. The fit of the dimer model to the experimental data was done in two ways using a nonlinear least-squares method and the procedure described in Ref. 35. Firstly, the model was fitted separately to each component of the doublet structure and the following dimensionless EMV-coupling constants were obtained: for $[\text{Pd}(\text{ddd})_2]_2\text{SbF}_6$ salt $\lambda(1193 \text{ cm}^{-1})=0.17$ and $\lambda(1154 \text{ cm}^{-1})=0.24$; for $[\text{Pd}(\text{ddd})_2]_2\text{AuBr}_2$ salt $\lambda(1196 \text{ cm}^{-1})=0.15$ and $\lambda(1154 \text{ cm}^{-1})=0.21$; nevertheless the fit was rather unsatisfactory. Subsequently, we introduced to the model an additional phonon mode at 1175 cm^{-1} to simulate the low-frequency component of the doublet structure and performed calculation using the same parameters describing electronic transitions as in the first method. This approach gave much better agreement with experimental reflectance: the suitable parameters are listed in Table IV and the fit qualities are shown in Fig. 12. Both calculations gave similar values of the EMV-coupling constants for the high-frequency component of the doublet struc-

ture, therefore, we believe that this is a proper estimation of the parameter describing the EMV coupling for C=C mode of $\text{Pd}(\text{ddd})_2$. The EMV-coupling constant for the low-frequency component is probably larger as results from the calculation using the first approach. Nevertheless, we want to emphasize that our analysis in terms of the dimer model is to be considered as a preliminary approach, since a proper model should generate the doublet structure. The work is under progress.

V. CONCLUSIONS

In this paper, we have presented and discussed the infrared spectra of three $\text{Pd}(\text{ddd})_2$ charge-transfer salts in which $\text{Pd}(\text{ddd})_2$ donors are arranged to form strongly dimerized stacks. A systematic analysis of the spectra allowed us to obtain important information about the electronic structure and various interactions in these organic conductors. Although the compounds show metallic-like behavior at room temperature, the spectral studies revealed the energy gaps in electronic excitation spectra. The charge-transfer features confirm the existence of two-band electronic structure. In all the salts, due to the short-range electron-electron and electron-phonon interactions, the low-energy electronic dispersion deviates strongly from a simple Drude-Lorentz model. Average transfer integrals were derived for the directions both parallel and perpendicular to the $\text{Pd}(\text{ddd})_2$ stacks. Our data confirm that the crystals are two-dimensional conducting salts in which side-by-side interactions between the neighboring stacks exceed those of face-to-face type between the dimers in stacks. Spectral features related to the electron-molecular vibration-coupling phenomena were analyzed in terms of the dimer model and suitable coupling constants were estimated. The origin of doublet structure of the C=C vibrational bands is discussed in terms of the coupling with LUMO and HOMO electrons. Our spectral data prove that the electronic charge-transfer excitations in $\text{Pd}(\text{ddd})_2$ salts should be studied in more detail.

ACKNOWLEDGMENTS

We thank L.A. Kushch for high-quality single crystals. We are greatly indebted to Dr. M. Połomska for help in FT-NIR Raman measurements and to O.A. Drozdova for reflectance measurements in the visible spectral range. One of us (A.Ł.) acknowledges the Foundation for Polish Science for support.

*Electronic address: lapinski@ifmpan.poznan.pl

¹H. Moril, *Int. J. Mod. Phys. B* **8**, 1 (1994).

²C.T. Vance, R.D. Bereman, J. Bordner, W.E. Hatfield, and J.H. Helms, *Inorg. Chem.* **24**, 2905 (1985).

³A.J. Schultz, H.H. Wang, L.C. Soderholm, T.L. Sifter, J.M. Williams, K. Bechgaard, and M.-H. Whangbo, *Inorg. Chem.* **26**, 3757 (1987).

⁴E.B. Yagubskii, A.I. Kotov, L.I. Buravov, A.G. Khomenko, V.E. Shklover, S.S. Nagapetyan, Yu.T. Struchkov, L.V. Vetoshkina, and L.Yu. Ukhin, *Synth. Met.* **35**, 271 (1990).

⁵E.B. Yagubskii, A.I. Kotov, E.E. Laukhina, A.A. Ignatiev, L.I. Buravov, A.G. Khomenko, V.E. Shklover, S.S. Nagapetyan, and Yu.T. Struchkov, *Synth. Met.* **41/43**, 2515 (1991).

⁶E.B. Yagubskii, A.I. Kotov, E.E. Laukhina, A.A. Ignatiev, A.G. Khomenko, S.S. Nagapetyan, V.E. Shklover, Yu.T. Struchkov, L.V. Vetoshkina, and L.Yu. Ukhin, *Mater. Sci.* **17**, 55 (1991).

⁷E.B. Yagubskii, A.I. Kotov, A.G. Khomenko, L.I. Buravov, and A.I. Schegolev, *Synth. Met.* **46**, 255 (1992).

⁸C. Faulmann, P. Cassoux, E.B. Yagubskii, and L.V. Vetoshkina, *New J. Chem.* **17**, 385 (1993).

- ⁹E.B. Yagubskii, L.A. Kushch, V.V. Gritsenko, O.A. Dyachenko, L.I. Buravov, and A.G. Khomenko, *Synth. Met.* **70**, 1039 (1995).
- ¹⁰L.A. Kushch, V.V. Gritsenko, L.I. Buravov, A.G. Khomenko, G.V. Shilov, O.A. Dyachenko, V.A. Merzhanov, E.B. Yagubskii, R. Rousseau, and E. Canadell, *J. Mater. Chem.* **5**, 1633 (1995).
- ¹¹L.A. Kushch, S.V. Konovalikhin, L.I. Buravov, A.G. Khomenko, G.V. Shilov, K. Van, O.A. Dyachenko, E.B. Yagubskii, C. Rovira, and E. Canadell, *J. Phys. I* **6**, 1555 (1996).
- ¹²A. Kobayashi and H. Kobayashi in *Handbook of Organic Conductive Molecules and Polymers* edited by H.S. Nalwa (J Wiley, New York 1997), Vol. 1, pp. 249–251.
- ¹³E. Canadell, E.-I. Rachidi, S. Ravy, J.P. Pouget, L. Brossard, and J.P. Legros, *J. Phys. (France)* **50**, 2967 (1989).
- ¹⁴E. Canadell, S. Ravy, J.P. Pouget, and L. Brossard, *Solid State Commun.* **75**, 633 (1990).
- ¹⁵M.-L. Doublet, E. Canadell, J.P. Pouget, E.B. Yagubskii, J. Ren, and M.-H. Whangbo, *Solid State Commun.* **88**, 699 (1993).
- ¹⁶E. Canadell, *Synth. Met.* **70**, 1009 (1995).
- ¹⁷H. Tajima, J. Shiraishi, and M. Kohomoto, *Solid State Commun.* **103**, 545 (1997).
- ¹⁸R. Bozio and C. Pecile, in *Spectroscopy of Advanced Materials*, edited by R.J.H. Clark and R.E. Hester (Wiley, Chichester 1990), pp.1-86.
- ¹⁹M.G. Kaplunov, A.I. Kotov, and E.B. Yagubskii, *Synth. Met.* **44**, 213 (1991).
- ²⁰R. Świetlik, N.D. Kushch, L.A. Kushch, and E.B. Yagubskii, *Phys. Status Solidi B* **181**, 499 (1994).
- ²¹R. Świetlik, L.A. Kushch, and E.B. Yagubskii, *Synth. Met.* **70**, 1053 (1995).
- ²²A. Łapiński, R. Świetlik, and N.D. Kushch, *Adv. Mater. Opt. Electron.* **6**, 321 (1996).
- ²³R.P. Shibaeva, S.S. Khasanov, B.Z. Narimbetov, L.P. Rozenberg, L.A. Kushch, and E.B. Yagubskii, *Kristallografiya* **43**, 1 (1998) [*Crystallogr. Rep.* **43**, 237 (1998)].
- ²⁴R.P. Shibaeva (private communication).
- ²⁵M.G. Kaplunov and R.N. Lyubovskaya, *J. Phys. I* **2**, 1811 (1992).
- ²⁶H.H. Wang, S.B. Fox, E.B. Yagubskii, L.A. Kushch, A. Kotov, and M.-H. Whangbo, *J. Am. Chem. Soc.* **119**, 7601 (1997).
- ²⁷A. Graja, in *Organic Conductors — Fundamentals and Applications*, edited by J.-P. Fargés (Dekker, New York, 1994), pp. 229–67.
- ²⁸H.L. Liu, D.B. Tanner, A.E. Pullen, K.A. Abboud, and J.R. Reynolds, *Phys. Rev. B* **53**, 10 557 (1996).
- ²⁹C.S. Jacobsen, *J. Phys. C* **19**, 5643 (1986).
- ³⁰C.S. Jacobsen, J.M. Williams, and H.H. Wang, *Solid State Commun.* **54**, 937 (1985).
- ³¹F. Wooten, *Optical Properties of Solids* (Academic, New York, 1972).
- ³²J.E. Eldridge, C.C. Homes, J.M. Williams, A.M. Kini, and H.H. Wang, *Spectrochim. Acta A* **51**, 947 (1995).
- ³³R. Ramakumar, Y. Tanaka, and K. Yamaji, *Phys. Rev. B* **56**, 795 (1997).
- ³⁴V.M. Yartsev and R. Świetlik, *Rev. Solid State Sci.* **4**, 69 (1990).
- ³⁵M.J. Rice, V.M. Yartsev, and C.S. Jacobsen, *Phys. Rev. B* **21**, 3437 (1980).